Asymmetric Coupled-Resonator Bandpass Filter for Ultra-Wide Stopband Rejection

Narayanan PRITHA [1,2], *Shanmugam MAHESWARI* [1]

[1] Dept. of Electronics and Communication Engineering, Panimalar Engineering College, Chennai, India
[2] Faculty of Information and Communication Engineering, Anna University, Chennai, India

prithabe28@gmail.com, maheswarisp@yahoo.co.in

Submitted July 2, 2025 / Accepted December 19, 2025 / Online first January 20, 2026

Abstract. *The research presents a novel combination of an asymmetric coupling with a stepped impedance resonator (ACSIR) to realize high performance bandpass filter, especially an ultra-wide stopband rejection. A basic second-order bandpass filter was developed and subsequently extended to a fourth-order configuration to improve key performance metrics, including wide stopband characteristics and compact size, without compromising insertion loss. The use of asymmetric coupling enables optimization of the filter response while preserving a simple configuration. Furthermore, the resonance conditions associated with the asymmetric coupling were examined through mathematical analysis. The proposed ACSIR filter achieved an enhanced fractional bandwidth (FBW) of 15.4%, a low insertion loss of 0.64 dB, and wide stopband rejection extending up to* $7.25 f_0$ *tailored for WLAN applications operating at 2.45 GHz.*

Keywords

Stepped impedance resonator, asymmetric coupled-resonator, bandpass filter, ultra-wide stopband rejection

1. Introduction

Bandpass filters play a crucial role in enhancing the performance, reliability, and efficiency of WLAN systems, making them an essential component in wireless communication technologies. Traditional filter designs often face challenges in meeting performance requirements while adhering to size constraints, as modern devices continue to miniaturize while demanding wider bandwidth, wide stopband and lower loss.

The equivalent circuit of a two-port network and the impedance or admittance parameters of a uniformly coupled four-port network in a microstrip inhomogeneous medium as investigated in [1], [2] respectively. The coupling relationship and design equations for non-symmetric coupled lines with unequal characteristic impedances are discussed in [3]. The transmission line model presented in [4] establishes a relationship between the position of transmission zeros and the tapping configuration, distinguishing between symmetric and asymmetric tapping points. Several popular hairpin resonator configurations are presented in [5–7] and [8–10], focusing on design methodologies involving impedance and electrical length ratios. Additionally, power handling capabilities are analyzed in [11–14], while parallel coupled lines with open stubs are explored in [15], [16] to achieve high selectivity and a wide stopband.

Various symmetrical filter structures have been proposed, including high- and low-impedance triple coupled lines [17], coupled ring resonators sandwiched between input and output feed lines [18], cross-shaped resonators with open or shorted parallel coupled lines [19], and double-folded hairpin lines with a cross-coupled configuration [20]. Additional designs include microstrip slot lines with coplanar waveguide structures [21] and substrate integrated waveguide cavities with rectangular slots [22], all featuring complex layout topologies with potential for further stopband enhancement.

Inline microstrip bandpass filter described in [23] uses various cross-couplings for introducing transmission zeros. Wide upper stopband is obtained by quarter-wave stepped-impedance resonators at the expense of high insertion loss. Hairpin structured filter [24], serial and parallel resonators tuned filter [25], and dumbbell-shaped defected ground structures (DGSs) based filter [26] offer improved filtering at the cost of increased size.

The filter designed for GNSS applications, as described in [27], stepped-impedance resonator folded structure using SISL technology is presented in [28], Y-shaped dual-band bandpass filter (DBBPF) in [29], cascaded coupled lines in [30], and parallel-coupled line based filter [31], were used to improve passband characteristics and selectivity by effectively introducing transmission zeros. A coupled lines topology in [32], quasi-reflectionless BPF [33] and T-shaped line coupled with SIR [34] were utilized to get wide bandwidth by compromising its circuit size.

The present study overcomes the limitations of previous research studies by proposing a novel combination of asymmetric coupling with stepped impedance resonators (SIRs). The SIR structure offers effective control over harmonic suppression and compact size. Asymmetric coupling, on the other hand, played a significant role in enhancing key performance metrics, particularly by enabling low insertion

DOI: 10.13164/re.2026.0075

loss and wide bandwidth. The resonance conditions associated with asymmetric coupling were analyzed in detail in this work. Building on these insights, a second-order bandpass filter was developed. It was further extended to a fourth-order configuration, offering wider stopband and reduced size, without compromising insertion loss. By leveraging the complementary characteristics of asymmetric coupling and SIRs, the proposed filter achieves two-stage miniaturization, enhanced stopband and low insertion loss.

2. Stepped Impedance Resonator with Asymmetric Coupling

In this context, the significance of asymmetric coupling is highlighted, along with its structural representation.

2.1 Second Order SIR with Asymmetric Coupling

In order to design proposed filter, a basic half-wavelength stepped impedance resonator is developed, as shown in Fig. 1. The impedances and electrical lengths associated with the two sections of the resonator are Z_1, Z_2, θ_1 and θ_2 respectively.

The fundamental resonance and the first spurious signal of the resonator are given in (1),

$$\tan\theta_1 = -\cot\theta_1 = \frac{Z_2}{Z_1}\cot\theta_2 \cdot \tag{1}$$

The SIR is designed for a fixed fundamental resonance, while the spurious frequencies can be varied by selecting different values of $u = \theta_1/(\theta_1+\theta_2)$ and $R = Z_2/Z_1$ as depicted in Fig. 2. The obtained resonator parameters at 2.4 GHz are $Z_1 = 78\ \Omega$, $Z_2 = 33\ \Omega$, $\theta_1 = 38$ deg, and $\theta_2 = 24$ deg.

Basically, stepped impedance resonators are coupled to lines of the same impedance (low-low or high-high impedances), forming symmetric coupled lines to achieve a BPF response. In contrast, asymmetric coupled lines involve coupling between different impedance lines (low-high or high-low). To realize this, two stepped-impedance resonators are connected in a configuration that enables coupling between unequal impedance lines, thereby producing asymmetric coupling. This introduced coupling interacts symmetrically with both sides of the resonators, resulting in the formation of a new resonator structure.

An asymmetric coupled-line analysis in an inhomogeneous medium begin with impedance matrix of a four-port network, obtained from the port current-voltage relationships. The lossless coupled-lines system is characterized by z_1 and z_2, the self-impedance per unit length of lines 1 and 2, and z_m, the mutual impedance between the lines. The normal-mode parameters such as propagation constants and voltage ratios, are represented by γ_c and γ_π, and R_c and R_π, respectively, which are derived from the eigenvalues and eigenvectors of the system. Z_1 and Z_2 denote the characteristics impedances of the uncoupled lines 1 and 2, respectively. The

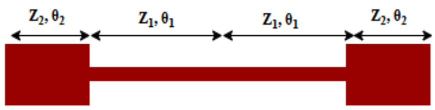

Fig. 1. Stepped impedance resonator.

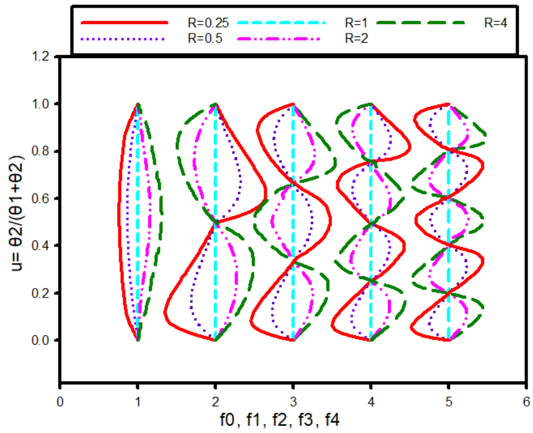

Fig. 2. Resonance of SIR.

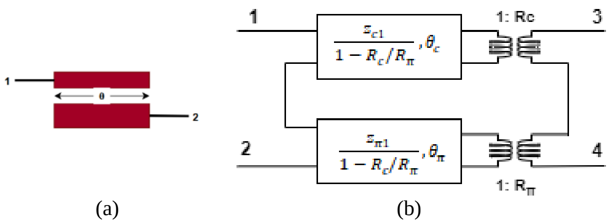

Fig. 3. (a) Structure; (b) Equivalent circuit of open-circuited inter-digital section.

quantities Z_{c1}, Z_{c2}, $Z_{\pi1}$, and $Z_{\pi2}$ correspond to the characteristics impedances of lines 1 and 2 for the C and π modes, as given in [2].

In the proposed design, the open-circuited interdigital two-port section shown in Fig. 3 is obtained from the four-port network by setting $I_2 = 0$ and $I_4 = 0$. The resulting impedance parameters for a homogeneous medium given in [2] are rewritten for the inhomogeneous medium, as presented in (2)–(4):

$$Z_{11} = -\mathrm{j}/2(Z_1/Z_2)^{1/2}\left(Z_{c1}\cot\theta_c + Z_{\pi1}\cot\theta_\pi\right), \tag{2}$$

$$Z_{13} = Z_{31} = -\mathrm{j}/2\left(Z_{c1}\theta_c + Z_{\pi1}\csc\theta_\pi\right), \tag{3}$$

$$Z_{33} = -\mathrm{j}/2(Z_2/Z_1)^{1/2}\left(Z_{c1}\cot\theta_c + Z_{\pi1}\cot\theta_\pi\right). \tag{4}$$

The design steps are summarized as follows:

1. Select the desired center frequency (f_0) and substrate, and determine the initial dimensions.
2. Calculate the impedances per unit length by considering the line widths and spacing using quasi-static analytical formula.
3. Obtain the eigenvalues and eigenvectors to determine the propagation constant of the modes.
4. Use the eigenvalues to compute the modal impedances and the eigenvectors to determine the voltage ratios.
5. Finally, use the obtained parameters to calculate the resonance of the filter.

$Z_{c1} = 121\ \Omega$	$Z_{\pi1} = 38.9\ \Omega$
$Z_{c2} = 55.5\ \Omega$	$Z_{\pi2} = 19.9\ \Omega$
$Z_1 = 78\ \Omega$	$Z_2 = 33\ \Omega$
$\varepsilon_{\text{eff,c}} = 1.78$	$\varepsilon_{\text{eff},\pi} = 2.05$

Tab. 1. Parameters of equivalent transmission line model.

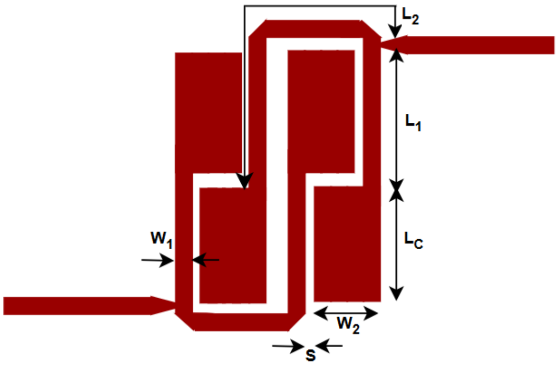

Fig. 4. Layout of ACSIR BPF. The dimensions are $L_1 = 6.2$ mm, $L_2 = 12.2$ mm, $L_C = 6$ mm, $W_1 = 1.1$ mm, $W_2 = 4.2$ mm and $S = 0.3$ mm.

Table 1 lists the appropriate values decided for the asymmetric-coupling based stepped-impedance resonators. These values are calculated starting from the initial dimensions of stepped impedance resonator and are further refined using the design procedure discussed earlier.

Figure 4 shows the stepped impedance bandpass filter with asymmetric coupling forming coupling between unequal characteristic impedance. The aim of the proposed ACSIR filter design leverages stepped impedance resonators that enable flexibility in impedance selection, allowing fine-tuning of bandwidth and resonance characteristics. Additionally, the asymmetric coupling facilitates an innovative means to control and optimize the filter's frequency response, contributing to the desired passband characteristics without increasing the overall size.

The asymmetric connection provides a comparatively longer coupling length than both end and symmetric coupling configurations. It employs both maximum coupling and maximum impedance transformation in a single architecture. Fine-tuning on coupling enables smooth adjustment of the bandwidth and allows filters to be more easily adapted to the desired operational frequency range, without altering the position of transmission zeros, unlike symmetric and end-coupling configurations. Thus, it resulted in finer control over both passband bandwidth and stopband parameters. Asymmetrical coupling facilitated the design of the more compact filter. Consequently, it enhances the overall performance of the system.

2.2 Fourth Order SIR with Asymmetric Coupling

Based on the achievements of the second-order design, a fourth-order configuration was developed for improving its stopband width and maintaining low insertion loss. This research, thus, contributes a practical and scalable solution to the design of bandpass filters, highlighting the effectiveness of stepped impedance and asymmetric coupling in achieving a compact footprint and high-quality filter response. The ACSIR filter offers a significant advancement in filter design, meeting the demands of the state-of-the-art communication systems for both performance and miniaturization.

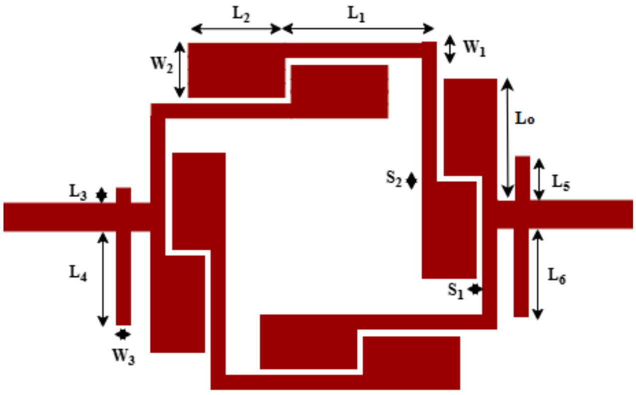

Fig. 5. Layout of the fourth order ACSIR BPF with open stubs. The layout dimensions are $L_1 = 9.2$ mm, $L_2 = 6$ mm, $L_0 = 8.5$ mm, $L_3 = 11.5$ mm, $L_4 = 12$ mm, $L_5 = 12$ mm, $L_6 = 12$ mm, $W_1 = 1.1$ mm, $W_2 = 4.2$ mm, $W_3 = 1$ mm, $S_1 = 0.3$ mm, $S_2 = 0.8$ mm.

The design was scaled to a higher-order configuration by employing four stepped impedance resonators, each asymmetrically coupled to the successive resonators. The fourth order stepped impedance resonator with asymmetric coupling and couple of open stub at the feed lines are shown in Fig. 5. The proposed bandpass filters are designed, simulated and tuned using Keysight ADS (Advanced Design System) 2020 full-wave electromagnetic simulator. Increasing the order of the filter enables the achievement of low insertion loss and sharp roll-off rate, which consequently improves the overall performance of the filter in addition to the signal integrity. The structure of coupling was optimized to reduce the design and fabrication complexity.

The roll-off rate and insertion loss (IL) increase with the order of the resonator (n), as expressed in (5) and (6):

$$\text{Roll-off rate} = 20 \times n \text{ (dB/decade)}, \tag{5}$$

$$\text{IL} = n \times \text{loss per resonator}. \tag{6}$$

The bandwidth (BW) narrows with higher order for the same ripple, indicating better frequency discrimination, as expressed in (7),

$$\text{BW} = 1/n. \tag{7}$$

The proposed filter has a consideration from the perspective of its geometry. Due to the resonator structure and coupling configuration, the physical layout may exhibit minor parasitic effects, such as unwanted coupling between adjacent sections, which can slightly shift the resonant frequencies. However, this consideration remain within acceptable ranges and is mitigated through careful layout optimization.

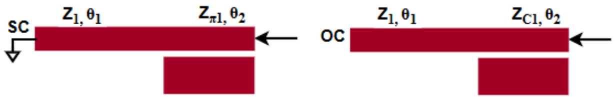

Fig. 6. (a) π mode circuit and (b) C mode circuit.

3. Resonance Conditions of ACSIR

The π and C πmode circuits of asymmetric coupled line are shown in Fig. 6(a) and Fig. 6(b), respectively. For simplicity, the coupled lines are considered as stubs during the analysis. Consequently, the π and C modes correspond to the odd and even modes of a general stepped impedance resonator structure.

3.1 Π Mode Analysis

Input impedance for π mode is

$$Z_{\text{in},\pi} = Z_{\pi 1} \frac{Z_{o1} + \text{j}Z_{\pi 1} \tan\theta_2}{Z_{\pi 1} + \text{j}Z_{o1} \tan\theta_2} \tag{8}$$

where

$$Z_{o1} = \text{j}Z_1 \tan\theta_1. \tag{9}$$

Substituting (9) in (8),

$$Z_{\text{in},\pi} = \text{j}Z_{\pi 1} \frac{(Z_{\pi 1} \tan\theta_2 + Z_1 \tan\theta_1)}{Z_{\pi 1} - Z_1 \tan\theta_1 \tan\theta_2}.$$

Equating $Z_{\text{in},\pi} = \infty$, then

$$Z_{\pi 1} - Z_1 \tan\theta_1 \tan\theta_2 = 0. \tag{10}$$

The resonant frequencies of π modes are,

$$\tan\theta_1 \tan\theta_2 = \frac{Z_{\pi 1}}{Z_1}. \tag{11}$$

Rewriting (11) as,

$$\tan\theta_1 \tan\theta_2 - \frac{Z_{\pi 1}}{Z_1} = 0. \tag{12}$$

By solving, π mode resonance frequency can be obtained.

3.2 C Mode Analysis

Input impedance for C mode is

$$Z_{\text{in,c}} = Z_{c1} \frac{Z_{o2} + \text{j}Z_{c1} \tan\theta_2}{Z_{c1} + \text{j}Z_{o2} \tan\theta_2}. \tag{13}$$

where

$$Z_{o2} = -\text{j}Z_1 \cot\theta_1. \tag{14}$$

Substituting (14) in (13)

$$Z_{\text{in},\pi} = -\text{j}Z_{c1} \frac{(Z_1 \cot\theta_1 - Z_{c1} \tan\theta_2)}{Z_{c1} + Z_1 \cot\theta_1 \tan\theta_2}..$$

Equating $Z_{\text{in,c}} = \infty$, then

$$Z_{c1} + Z_1 \cot\theta_1 \tan\theta_2 = 0. \tag{15}$$

The resonant frequencies of C mode is,

$$\cot\theta_1 \tan\theta_2 = -\frac{Z_{c1}}{Z_1}. \tag{16}$$

Rewriting (16) as,

$$\cot\theta_1 \tan\theta_2 + \frac{Z_{c1}}{Z_1} = 0. \tag{17}$$

By solving, C mode resonance frequency can be obtained.

The π and C mode resonance frequencies were derived using equations from (8) to (17) with 6 dB coupling between the coupled lines. With $L_1 = 12$ mm, $L_2 = 6$ mm, modal impedance ratio $Z_{\pi 1}/Z_1 = 0.44$, modal phase constant β_π and velocity $\upsilon_{p\pi}$, the π mode resonance frequency is obtained as 2.45 GHz using (12). Using the same lengths but different modal impedance ratio $Z_{C1}/Z_1 = 1.5$, modal phase constant β_C and velocity υ_{pc}, the C mode resonance frequency is obtained as 6.01 GHz using (17). Because $\upsilon_{p\pi} < \upsilon_{pc}$, the odd mode exhibits stronger field concentration, resulting in a higher effective permittivity. Consequently, the even mode resonance occurs at a higher frequency $f_\pi > f_C$. Stronger coupling leads to greater frequency separation between the fundamental and spurious resonances. This enhances the filter's spurious-free dynamic range.

3.3 Tapping Position

The tapping position of the feed lines are defined by (18) and (19). The tapping position refers to the point where energy is coupled into or out of the resonator.

$$\tan\theta_1 \tan\theta_c = \frac{Z_2}{Z_1}, \tag{18}$$

$$\tan\theta_2 \tan\theta_c = \frac{Z_2}{Z_1}. \tag{19}$$

The tapping position is typically chosen along the length of the resonator, which is often a quarter-wavelength ($\lambda/4$) or half-wavelength ($\lambda/2$) structure. The amount of energy coupled into or extracted from the resonator depends on the tapping position. At certain positions, the electric or magnetic field strength is maximum or minimum, corresponding to anti-nodes and nodes, respectively. Placing the tap near an anti-node (maximum field strength) results in stronger coupling, while placing it near a node (minimum field strength) results in weaker coupling. The tapping position affects the impedance seen by the input or output port of the designed filter as denoted in Fig. 4. Optimization helps in controlling the tapping position to achieve impedance matching for maximum power transfer or desired filter characteristics.

The simulated results of various tapping positions are as shown in Fig. 7. When tapping is placed at 0.33 $\lambda/2$ ($L = 9$ mm), perfect impedance matching, also maximum power transfer can be achieved. When tapping is placed at

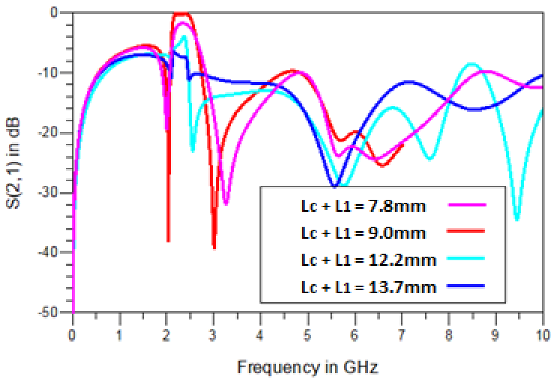

Fig. 7. Simulated results with various tapping position of ACSIR.

0.29 $\lambda/2$ (L = 7.8 mm) and 0.45 $\lambda/2$ (L = 12.2 mm), power loss occurs due to impedance mismatch between the source and load.

When the tapping position is fixed at the center of the stepped impedance resonator at $\lambda/2$ (L = 13.7 mm), the power null will get delivered to the load.

4. Results and Discussions

The substrate used was Rogers RT 5870 with ε_r of 2.33, h of 0.785 mm and dielectric loss tangent of 0.0012. The simulated results were obtained using ADS momentum and measurement carried out by E5062A vector analyzer.

The response of second-order asymmetric coupling filter is shown in Fig. 8, indicating a 3 dB bandwidth ranging from 2.1 to 2.6 GHz, with a fractional bandwidth of 20% and a center frequency of 2.45 GHz. The transmission zeros at 2 GHz and 3 GHz indicate the filter's selectivity.

A shape factor of 1.8 is achieved, along with excellent in-band performance, demonstrated by an insertion loss (S_{21}) of 0.2 dB and a return loss (S_{11}) of 24 dB. However, the stopband rejection is limited to 6 dB in the lower stopband and 10 dB in the upper stopband, primarily due to the second-order filter design. Despite this limitation, the key parameters indicate efficient overall performance, with the exception of stopband suppression.

The analysis of fourth order BPF with asymmetric coupling is discussed further. As the coupling length between

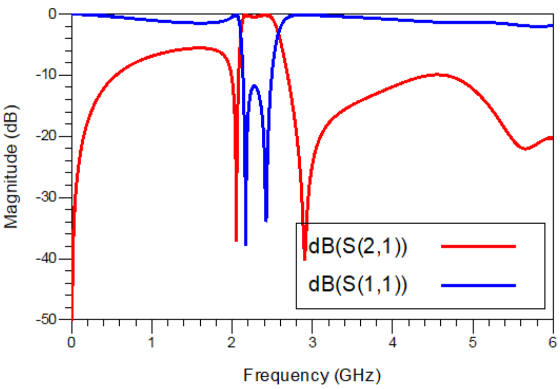

Fig. 8. Response of basic ACSIR BPF.

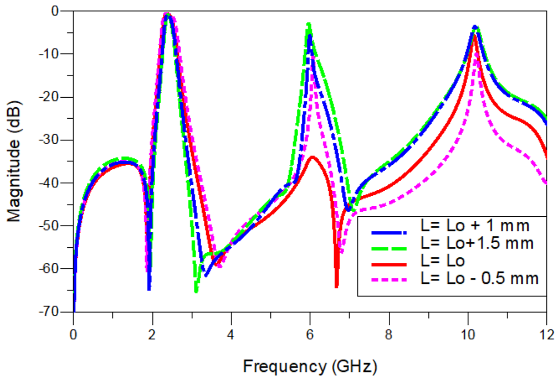

Fig. 9. Comparison of ACSIR BPF with various coupling length L.

adjacent resonators is increased in steps of 0.5 mm, the second harmonic appears in all cases except when the length L_0 is 8 mm. A wide bandwidth can be achieved, with only a slight shift in the transmission zeros, while maintaining the same level of insertion loss. As shown in Fig. 9, the coupling length between the resonators significantly influenced the suppression of spurious signals and the rejection level in the upper stopband.

As the coupling gap increases from 0.3 mm to 0.9 mm in increments of 0.3 mm, a corresponding increase in bandwidth is observed, along with a slight shift in the transmission zeros, as shown in Fig. 10. Variations in the coupling gap also influence key parameters such as fractional bandwidth, shape factor, the position of transmission zeros in the lower band, and the rejection level in the upper stopband.

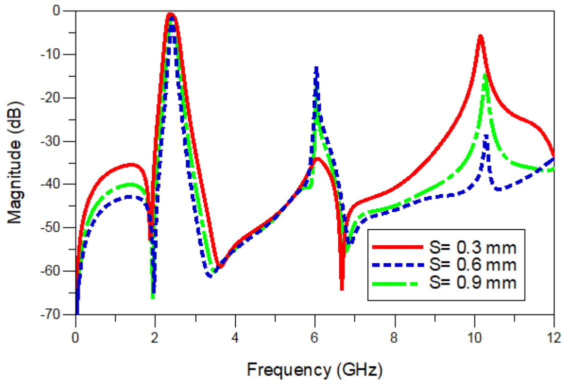

Fig. 10. Comparison of ACSIR BPF with various coupling gap S.

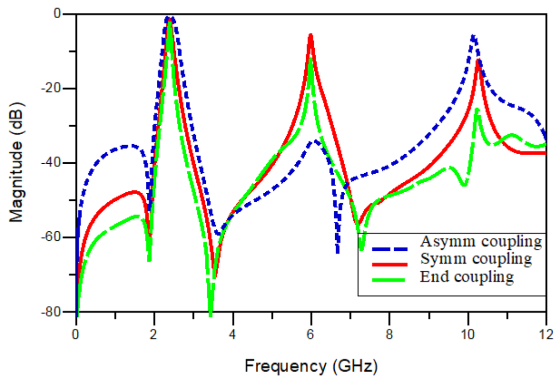

Fig. 11. Comparison of S_{21} between end, symmetric and asymmetric coupling.

The comparison in magnitude responses of insertion loss between end coupling, symmetric coupling, and asymmetric coupling is shown in Fig. 11. From the observation of the response, asymmetric coupling resulted in a notably low insertion loss and wide bandwidth.

The transmission zeros were visibly shifted away from their positions in the end-coupling configuration. Additionally, the rejection level in the upper band was improved, effectively suppressing second harmonics when asymmetric coupling was employed in the design.

From the magnitude response of S_{11}, it is observed that the return loss is significantly deeper in the asymmetric coupling configuration compared to other coupling types. As shown in Fig. 12, the loss remains below one at the second harmonic, indicating effective rejection at that frequency when asymmetric coupling is applied.

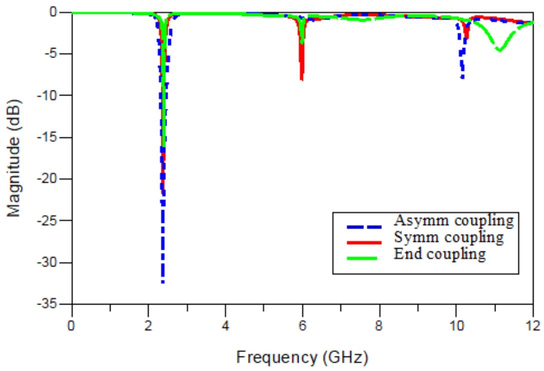

Fig. 12. Comparison of S_{11} between end, symmetric and asymmetric coupling.

Design	FBW (%)	IL (dB)	HS (20 dB Attn. GHz)	Size $\lambda_g \times \lambda_g$
End coupling	1	2.2	5.9	0.37 × 0.37
Symmetric coupling	2.9	1.27	5.78	0.35 × 0.35
Asymmetric coupling	20	0.42	9.8	0.25 × 0.25

Tab. 2. Comparison of simulated responses (HS-harmonic suppression, FBW- fractional bandwidth).

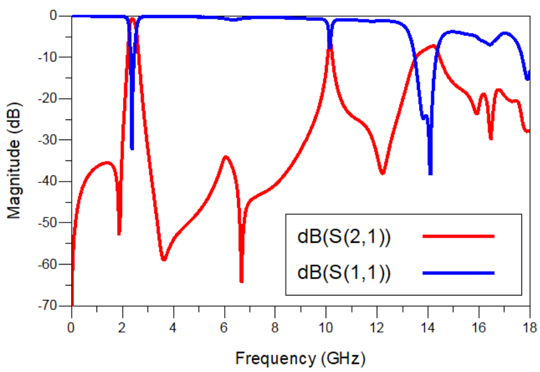

Fig. 13. Simulated response of fourth order ACSIR BPF without open stubs.

From Tab. 2, types of couplings and their parameters can be gathered. End coupling, symmetric coupling, and asymmetric coupling were compared, and it can be concluded that asymmetric coupling is proven to be the most effective choice for achieving low insertion loss, wide fractional bandwidth (FBW), and compact filter size.

The simulated response of fourth order asymmetric coupling BPF without open stubs at the feedline can be seen in Fig. 13.

At center frequency of 2.45 GHz, insertion loss of 0.42 dB and return loss of 39.2 dB was noted. The stepped impedance resonator introduced in the design with selected impedance and electrical length ratio, second order (6.01 GHz) and fifth order (17.93 GHz) spurious signals were rejected. Thus, an out-of-band attenuation of 20 dB was observed up to a frequency of 9.8 GHz (3.55 f_0). To enhance the rejection in stopband, open stubs with desired lengths were incorporated.

The simulated response of fourth order asymmetric coupling BPF with open stubs can be seen in Fig. 14. The simulated odd and even mode resonance frequencies were 2.45 GHz and 6.01 GHz, and the transmission zeros were at 2 and 3.8 GHz. In order to achieve good out-of-band response, the fourth order resonator structure and the open stubs were introduced at feed line.

From the analysis of the response of fourth order asymmetric coupling BPF with open stubs, good insertion loss of 0.52 dB and return loss of 24.13 dB were observed. The established stubs rejected higher mode spurious signals from second order (6.51 GHz), third order (11.12 GHz), fourth order (15.18 GHz), and fifth order (17.93 GHz). Enhanced out-of-band attenuation of 20 dB was achieved up to 19.64 GHz (7.25 f_0), with further 15 dB attenuation beyond 27 GHz (10 f_0).

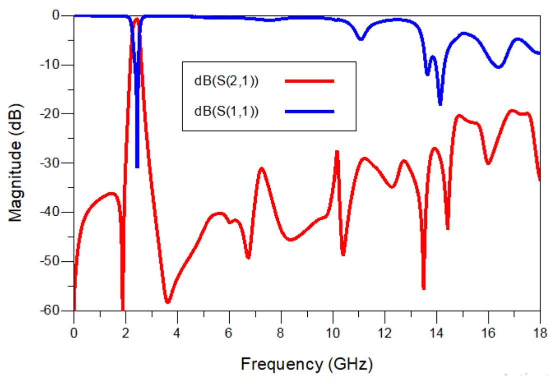

Fig. 14. Simulated response of fourth order ACSIR BPF with open stubs.

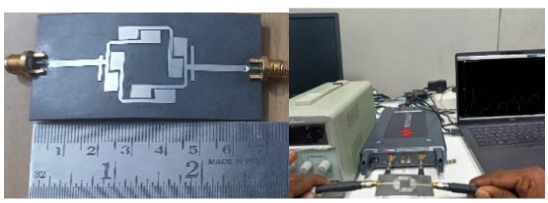

Fig. 15. Photograph of proposed filter with measurement setup.

Ref	f_0 (GHz)	IL (dB)	RL (dB)	FBW (%)	Spurious signal	Size $\lambda_g \times \lambda_g$
[17]	2.4	1.2	15	12.1	$2.5f_0$ (20 dB)	0.28 × 0.16
[18]	2.1	1.8	> 12	19	$3f_0$ (18 dB)	0.39 × 0.28
[19]-I	2.9	0.7	12	10.4	–(15 dB)	0.2 × 0.2
[20]	2.5	1.2	25	4	$3.76f_0$ (35 dB)	0.22 × 0.27
[21]	2.94	< 0.5	≥ 18.3	116.4	$3f_0$ (18.53 dB)	0.73 × 0.51
[22]-I	0.87	0.7	23.63	15.7	$3.86f_0$ (20 dB)	0.036 λ_g^2
[23]	1	2.6	15	20	$3.98f_0$ (30 dB)	0.11 × 0.06
[24]	2	1.3	11.3	-	$10f_0$ (32 dB)	0.64 × 0.43
[25]	2.45	0.798	22.7	10	-	0.92 × 0.34
[26]	6	-	18	63	$2.8f_0$ (25 dB)	0.62 × 0.19
This work	2.45	0.64	18.5	15.4	$7.25f_0$ (20 dB) $10f_0$ (15 dB)	0.25 × 0.25

Tab. 3. Comparison of previous works with the proposed work.

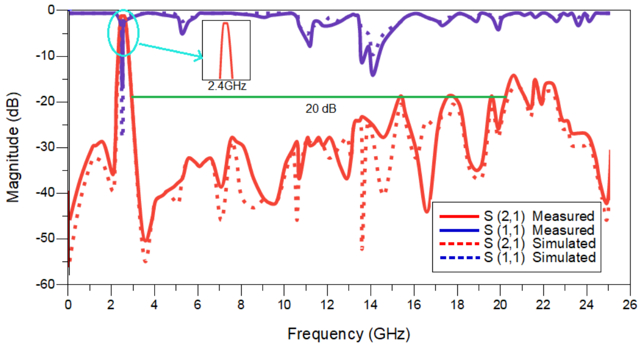

Fig. 16. Response of simulated and measured responses.

In Fig. 15, the left side displays a photograph of the fabricated filter, and the right side shows the measurement setup. The measurements were performed with the aid of vector analyzer, and the output depicting both simulated and measured responses of S_{11} and S_{21} as shown in Fig. 16.

As observed, the measured S_{11} at the center frequency drops to 18.5 dB, compared to the simulated value of 24.13 dB, primarily due to reflections during measurement. As expected, the measured S_{21} response closely aligned with the simulated results, ranging from 0.52 dB to 0.64 dB.

Higher-order bandpass filters with asymmetric coupling leveraged these benefits to deliver superior performance, adaptability, and efficiency in a wide range of communication applications. The measured parameters of various works with proposed work are compared as depicted in Tab. 3. The proposed fourth order stepped impedance resonator with asymmetric coupling is designed at 2.4 GHz, focused to deliver low insertion loss of 0.64 dB and better return loss of 18.5 dB.

The miniaturization in filter size of $0.25\,\lambda_g \times 0.25\,\lambda_g$ and better out of band attenuation was achieved with 20 dB till frequency of 19.64 GHz (7.25 f_0), further 15 dB attenuation more than 27 GHz (10 f_0) was also achieved. Also, narrow band with fractional bandwidth of 15.4% was measured from the response. The comparison confirmed that the stepped impedance resonator with asymmetric coupling is a superior choice for achieving low insertion loss, high return loss, narrow bandwidth, compact size, and excellent out-of-band attenuation, effectively rejecting spurious signals from the second to the sixth harmonic. The results demonstrated that the ACSIR filter performs as intended, offering low insertion loss and a compact footprint, thereby validating its suitability for practical applications.

5. Conclusion

This work presents a bandpass filter based on an asymmetric coupling with stepped impedance resonator. The incorporation of asymmetric coupling proved critical in minimizing insertion loss and enabling precise passband control without increasing the filter's physical footprint. Additionally, careful impedance selection within the resonator allows fine-tuning of bandwidth and resonance frequencies. The successful design and validation of both second- and fourth-order configurations confirmed the scalability and adaptability of the ACSIR filter for applications demanding a wide stopband and high performance in compact spaces. This two-tiered approach, combining impedance optimization with innovative coupling techniques, demonstrated strong potential for advancing miniaturized RF component design.

References

[1] JOHNSON, A. K., ZYSMAN, G. I. Coupled transmission line networks in an inhomogeneous dielectric medium. *IEEE Transactions on Microwave Theory and Techniques*, 1969, vol. 17, no. 10, p. 753–759. DOI: 10.1109/TMTT.1969.1127055

[2] TRIPATHI, V. K. Asymmetric coupled transmission lines in an inhomogeneous medium. *IEEE Transactions on Microwave Theory and Techniques*, 1975, vol. 23, no. 9, p. 735–739. DOI: 10.1109/TMTT.1975.1128665

[3] CRISTAL, E. G. Coupled transmission line directional couplers with coupled lines of unequal characteristics impedances. *IEEE*

Transactions on Microwave Theory and Techniques, 1966, vol. 14, no. 7, p. 337–346. DOI: 10.1109/TMTT.1966.1126266

[4] HSIEH, L. H., CHANG, K. Tunable microstrip bandpass filters with two transmission zeros. *IEEE Transactions on Microwave Theory and Techniques*, 2003, vol. 51, no. 2, p. 520–525. DOI: 10.1109/TMTT.2002.807830

[5] LEE, S. S., TSAI, C. New cross-coupled filter design using improved hairpin resonators. *IEEE Transactions on Microwave Theory and Techniques*, 2000, vol. 48, no. 12, p. 2482–2490. DOI: 10.1109/22.899002

[6] HONG, J. S., LANCASTER, M. J. *Microstrip Filters for RF/Microwave Applications*. New York (USA): John Wiley & Sons, 2001. ISBN: 0-471-38877-7

[7] HSIEH, L. H., CHANG, K. Compact elliptic-function low-pass filters using microstrip stepped-impedance hairpin resonators. *IEEE Transactions on Microwave Theory and Techniques*, 2003, vol. 51, no. 1, p. 193–199. DOI: 10.1109/TMTT.2002.806901

[8] CHEN, X., ZHANG, L., PENG, Y., et al. Compact lowpass filter with wide stopband bandwidth. *Microwave and Optical Technology Letters*, 2015, vol. 57, no. 2, p. 367–371. DOI: 10.1002/mop.28853

[9] YANG, M. H., XU, J. Design of compact, broad-stopband lowpass filter using modified stepped impedance hairpin resonators. *Electronics Letters*, 2008, vol. 44, no. 20, p. 1198–1200. DOI: 10.1049/el:20081875

[10] ZHOU, L., LONG, Z., LI, H., et al. Design of an ultrawide stopband HTS LPF based on interdigital hairpin structure. *IEEE Microwave and Wireless Components Letters*, 2018, vol. 28, no. 8, p. 666–668. DOI: 10.1109/LMWC.2018.2847462

[11] CHEN, C. F., HUANG, T. Y., WU, R. B., et al. Design of microstrip bandpass filters with multiorder spurious-mode suppression. *IEEE Transactions on Microwave Theory and Techniques*, 2005, vol. 53, no. 12, p. 3788–3793. DOI: 10.1109/TMTT.2005.859869

[12] LIN, S. C., LIN, Y. S., CHEN, C. H. Extended-stopband bandpass filter using both half- and quarter-wavelength resonators. *IEEE Microwave and Wireless Components Letters*, 2006, vol. 16, no. 1, p. 43–45. DOI: 10.1109/LMWC.2005.860014

[13] LIN, S. C., DENG, P. H., LIN, Y. S., et al. Wide-stopband microstrip bandpass filters using dissimilar quarter-wavelength stepped-impedance resonators. *IEEE Transactions on Microwave Theory and Techniques*, 2006, vol. 54, no. 3, p. 1011–1018. DOI: 10.1109/TMTT.2005.864139

[14] MORALES-HERNANDEZ, A., SANCHEZ-SORIANO, M. A., MARINI, S., et al. Increasing peak power handling in microstrip bandpass filters by using rounded-end resonators. *IEEE Microwave and Wireless Components Letters*, 2021, vol. 31, no. 3, p. 237–240. DOI: 10.1109/LMWC.2021.3050765

[15] HUNG, C. Y., WENG, M. H., YANG, R. Y., et al. Design of the compact parallel coupled wideband bandpass filter with very high selectivity and wide stopband. *IEEE Microwave and Wireless Components Letters*, 2007, vol. 17, no. 7, p. 510–512. DOI: 10.1109/LMWC.2007.899312

[16] SAGHIR, A., QUDDIOUS, A., ARAIN, S., et al. Single-/dual- BPF using coupled-line stepped impedance resonators (CLSIR). *IEEE Transactions on Circuits and Systems-II: Express Briefs*, 2019, vol. 66, no. 9, p. 1497–1501. DOI: 10.1109/TCSII.2018.2889846

[17] AFZALI, B., ABBASI, H., SHAMA, F., et al. A microstrip band-pass filter with deep rejection and low insertion loss for application at 2.4 GHz useful wireless frequency. *AEU-International Journal of Electronics and Communications*, 2021, vol. 138, p. 1–8. DOI: 10.1016/j.aeue.2021.153811

[18] XU, K. D., ZHANG, F., LIU, Y., et al. Bandpass filter using three pairs of coupled lines with multiple transmission zeros. *IEEE Microwave and Wireless Components Letters*, 2018, vol. 28, no. 7, p. 576–578. DOI: 10.1109/LMWC.2018.2835643

[19] LA, D. S., GUAN, X., WANG, M. Y., et al. Compact wideband bandpass filter based on coupled line stub with high selectivity. *AEU-International Journal of Electronics and Communications*, 2021, vol. 138, p. 1–6. DOI: 10.1016/j.aeue.2021.153872

[20] DAS, T. K., CHATTERJEE, S., RAHIM, S. K. A., et al. Compact high-selectivity wide stopband microstrip cross-coupled bandpass filter with spurline. *IEEE Access*, 2022, vol. 10, p. 69866–69882. DOI: 10.1109/ACCESS.2022.3187408

[21] CHAI, Y. Q., MO, J. R., HU, S. B., et al. Wideband Chebyshev bandpass filter with extended upper stopband using shunt short-ended slotline stubs. *IEEE Transactions on Circuits and Systems-II: Express Briefs*, 2022, vol. 69, no. 8, p. 3376–3380. DOI: 10.1109/TCSII.2022.3156549

[22] BARIK, R. K., KOZIEL, S. Compact, order extensible and wide-stopband bandpass filter based on SIW cavity with rectangular ring slot. *IEEE Transactions on Circuits and Systems-II: Express Briefs*, 2022, vol. 69, no. 12, p. 4784–4788. DOI: 10.1109/TCSII.2022.3196370

[23] TANG, S. C., CHU, P. C., KUO, J. T., et al. Compact microstrip wideband cross-coupled inline bandpass filters with miniaturized stepped-impedance resonators (SIRs). *IEEE Access*, 2022, vol. 10, p. 21328–21335. DOI: 10.1109/ACCESS.2022.3153710

[24] SHARIFI, M., MASHAYEKHI, V. Design of a modified hairpin bandpass filter using embedded radial stubs featuring ultrawide stopband. *AEU-International Journal of Electronics and Communications*, 2023, vol. 164, p. 1–9. DOI: 10.1016/j.aeue.2023.154624

[25] CHEN, S., SHI, L. F., LIU, G. X., et al. An alternate circuit for narrow-bandpass elliptic microstrip filter design. *IEEE Microwave and Wireless Components Letters*, 2017, vol. 27, no. 7, p. 624–626. DOI: 10.1109/LMWC.2017.2711528

[26] YUAN, W., LIU, X., LU, H., et al. Flexible design method for microstrip bandstop, highpass, and bandpass filters using similar defected ground structures. *IEEE Access*, 2019, vol. 7, p. 98453 to 98461. DOI: 10.1109/ACCESS.2019.2928816

[27] MAO, X., LIU, W., NAN, J. Design of a harmonic suppressed Dual-band reconfigurable bandpass filter for multistandard GNSS receivers. *IEEE Access*, 2022, vol. 10, p. 96788–96797. DOI: 10.1109/ACCESS.2022.3206005

[28] YUE, Z., MA, K., WANG, Y. Design of Ka-band SISL high selectivity bandpass filter with controllable zeros. *IEEE Microwave and Wireless Technology Letters*, 2023, vol. 33, no. 9, p. 1278 to 1281. DOI: 10.1109/LMWT.2023.3282636

[29] SHANKAR, E., PHANI KUMAR, K. V., VELIDI, V. K. Design of high selectivity compact dual-band bandpass filter with seven transmission-zeros for GPS and WiMAX applications. *IEEE Transactions on Circuits and Systems-II: Express Briefs*, 2023, vol. 70, no. 7, p. 2395–2399. DOI: 10.1109/TCSII.2023.3238792

[30] SHANKAR, E., PHANI KUMAR, K. V., VELIDI, V. K., et al. Miniaturized dual-band bandpass filter with wide inter stopband for 5G applications. *IEEE Transactions on Circuits and Systems-II: Express Briefs*, 2024, vol. 71, no. 10, p. 4461–4465. DOI: 10.1109/TCSII.2024.3395621

[31] VRYONIDES, P., ARAIN, S., QUDDIOUS, A., et al. A new class of high-selectivity bandpass filters with constant bandwidth and 5:1 bandwidth tuning ratio. *IEEE Access*, 2024, vol. 12, p. 16489 to 16497. DOI: 10.1109/ACCESS.2024.3358677

[32] PHANI KUMAR, K. V., VELIDI, V. K., RAJKUMAR, R., et al. A compact ultra-wideband multimode bandpass filter with sharp-rejection using stepped impedance open stub and series transformers. *IEEE Transactions on Circuits and Systems-II: Express Briefs*, 2022, vol. 69, no. 12, p. 4824–4828. DOI: 10.1109/TCSII.2022.3192512

[33] ZHANG, S., LIU, H., WANG, Z., et al. Design of wideband quasi-reflectionless filter with high selectivity and flat passband. *IEEE*

Transactions on Circuits and Systems-II: Express Briefs, 2023, vol. 70, no. 11, p. 4038–4042. DOI: 10.1109/TCSII.2023.3284420

[34] ARULAALAN, M., RAMASAMY, V., SARAVANAKUMAR, R., et al. Design of a triple-bandpass filter using a modified T-shaped rectangular coupled with a stepped impedance resonator for smart portable communication device application. *Materials and Technology*, 2023, vol. 57, no. 4, p. 309–316. DOI: 10.17222/mit.2023.846

About the Authors …

PRITHA Narayanan received M.E. degree in Applied Electronics from Sathyabama Institute of Science and Technology, Chennai in 2013. She received B.E. degree in ECE from Adhiparasakthi College of Engineering, Anna University. She is working as an Assistant Professor in the Department of Electronics and Communication Engineering at Panimalar Engineering College, specializing in RF and microwave engineering. Her research focuses on developing novel bandpass filter design for microwave and mm wave applications. She has published over 15 peer-reviewed articles in the field of ECE.

MAHESWARI Shanmugam received Ph.D. degree in Microwave Engineering and M.E. degree in Applied Electronics from Sathyabama Institute of Science and Technology, Chennai in 2016 and 2009 respectively. She received B.E. degree in ECE from University of Madras. Her area of research includes microwave and millimeter wave circuits. She has more than two decade of teaching experience. Currently she is working as a Professor in Panimalar Engineering College, Chennai. She is a recognized supervisor for doing research in Anna University. She has published more than 30 papers in Web of Science, Scopus indexed journals and IEEE conferences. She is a Fellow of IETE.